ARTICLES
https://doi.org/10.1038/s41566-020-0617-x

nature photonics

Photonic microwave generation in the X- and K-band using integrated soliton microcombs

Junqiu Liu[1,4], Erwan Lucas[1,4], Arslan S. Raja[1,4], Jijun He[1,2,4], Johann Riemensberger[1], Rui Ning Wang[1], Maxim Karpov[1], Hairun Guo[1,3], Romain Bouchand[1] and Tobias J. Kippenberg[1]✉

Microwave photonic technologies, which upshift the carrier into the optical domain, have facilitated the generation and processing of ultra-wideband electronic signals at vastly reduced fractional bandwidths. For microwave photonic applications such as radars, optical communications and low-noise microwave generation, optical frequency combs are useful building blocks. By virtue of soliton microcombs, frequency combs can now be built using CMOS-compatible photonic integrated circuits. Yet, currently developed integrated soliton microcombs all operate with repetition rates significantly beyond those that conventional electronics can detect, preventing their use in microwave photonics. Access to this regime is challenging due to the required ultra-low waveguide loss and large dimensions of the nanophotonic resonators. Here, we demonstrate soliton microcombs operating in two widely employed microwave bands, the X-band (~10 GHz, for radar) and the K-band (~20 GHz, for 5G). Driven by a low-noise fibre laser, these devices produce more than 300 frequency lines within the 3 dB bandwidth, and generate microwave signals featuring phase noise levels comparable to modern electronic microwave oscillators. Our results establish integrated microcombs as viable low-noise microwave generators. Furthermore, the low soliton repetition rates are critical for future dense wavelength-division multiplexing channel generation schemes and could significantly reduce the system complexity of soliton-based integrated frequency synthesizers and atomic clocks.

The synthesis, distribution and processing of radio and microwave signals is ubiquitous in our information society for radar, wireless networks and satellite communications. With the looming bandwidth bottleneck in telecommunications[1] (due to the future requirements of 5G and the Internet of Things, for example), the tendency is to use carriers in higher frequency bands. As it becomes progressively more difficult to generate and digitize electronic signals with increasing carrier frequency, the use of photonics to process ultra-wideband signals has been explored extensively. This is commonly referred to as 'microwave photonics'[2]. Landmark demonstrations of microwave photonics in filters[3], radar[4], analog-to-digital converters[5], radio-over-fibre[6], waveform generation[7], subnoise detection[8] and optical communications[9] have achieved a bandwidth not attainable using conventional electronics. Similarly, the synthesis of low-noise microwave signals, paramount in a large variety of modern applications (such as time–frequency metrology[10] and wireless broadband communications[11]), has attained unrivalled performance in terms of spectral purity (noise)[12–14] by using optical frequency division based on frequency combs. However, future deployment of these technologies critically depends on achieving similar performance enhancements with photonic integrated components[15]. In this context, integrated microresonator-based soliton frequency combs ('soliton microcombs')[16,17] could be key building blocks as sources of multiple coherent optical carriers for optical and microwave synthesis[18–20]. Silicon nitride (Si_3N_4)[21], a CMOS-compatible material with excellent power-handling capability[22], has given rise to photonic integrated microcombs, which operate in the dissipative Kerr soliton regime[23,24] with low power and can be integrated with compact lasers[25,26]. Further optical or electrical functionalities[27,28] can be co-integrated on chip. Recently, Si_3N_4-based soliton microcombs have been utilized in several system-level demonstrations[16], such as coherent communications, ultrafast ranging, astrophysical spectrometer calibration and optical coherence tomography, and could form the basis for integrated photonics-based microwave generation. However, the soliton formation threshold power increases with decreasing repetition rates. This unfavourable power scaling has prevented the repetition rates of integrated soliton microcombs from being reduced towards the microwave bands that can be processed easily by regular optoelectronic components.

So far, soliton microcombs with repetition rates in the microwave K- and X-bands ($f_{rep} < 20$ GHz) have been demonstrated only in low-refractive-index materials such as silica and bulk polished crystalline microresonators[14,29]. These microresonators can only operate with air cladding and thus have a limited capability for scalable manufacturing using CMOS foundry processes. Meanwhile, they are sensitive to contamination and are challenging to integrate with active tuning components such as piezoelectric actuators or metallic heaters[27,28]. For integrated platforms such as Si_3N_4, the main challenges hindering soliton generation at microwave repetition rates are related to the comparatively low quality (Q) factor and thermal effects. Laser powers of up to several watts are required to obtain microwave-repetition-rate solitons due to the decreasing Q caused by fabrication-related defects such as lithography stitching errors. For example, when using electron-beam lithography, stitching errors tend to accumulate in larger pattern areas, resulting in device failure and low fabrication yield for long waveguides or large rings. Complex resonator shapes have been utilized to avoid stitching errors[30,31], and 20 GHz free

[1]Institute of Physics, Swiss Federal Institute of Technology Lausanne (EPFL), Lausanne, Switzerland. [2]Department of Electrical Engineering, The Hong Kong Polytechnic University, Hong Kong, China. [3]Present address: Key Laboratory of Specialty Fiber Optics and Optical Access Networks, Joint International Research Laboratory of Specialty Fiber Optics and Advanced Communication, Shanghai Institute for Advanced Communication and Data Science, Shanghai University, Shanghai, China. [4]These authors contributed equally: Junqiu Liu, Erwan Lucas, Arslan S. Raja, Jijun He. ✉e-mail: tobias.kippenberg@epfl.ch

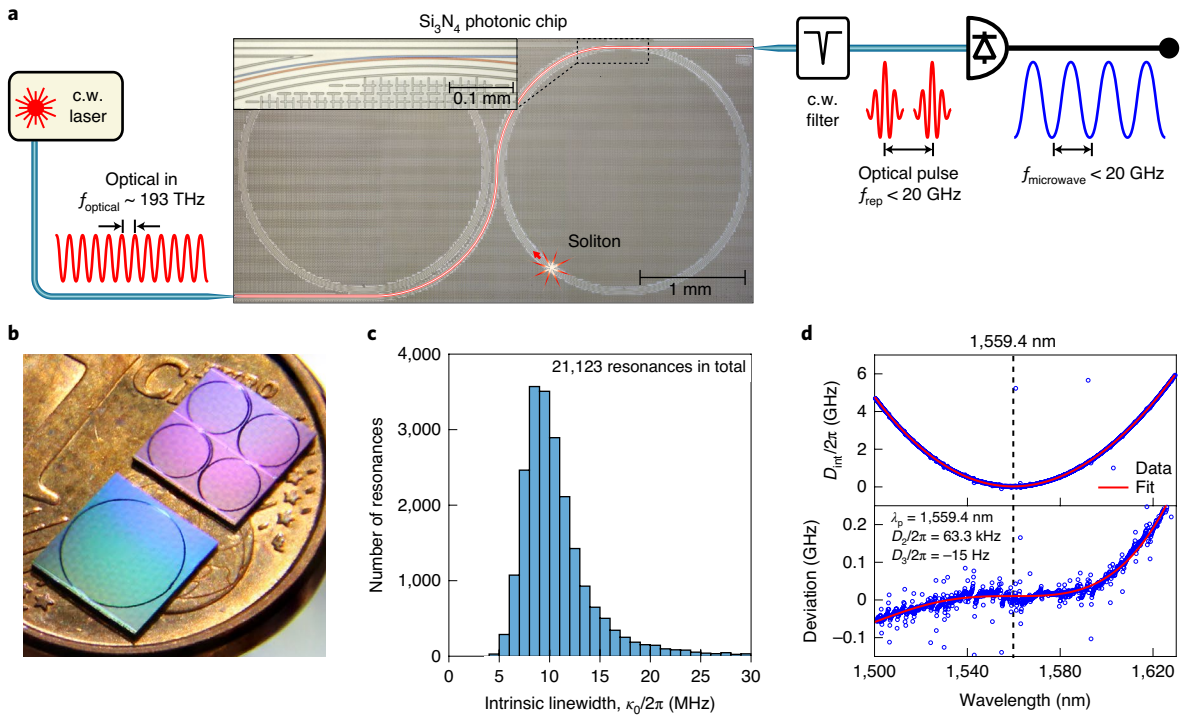

Fig. 1 | Principle of photonic microwave generation using integrated soliton microcombs and characteristics of the Si_3N_4 microresonators. a, Concept of microwave generation using an integrated Si_3N_4 soliton microcomb driven by a c.w. laser. The microscope image of the Si_3N_4 photonic chip highlights the bus-waveguide-to-ring-resonator coupling and the stress-release patterns to prevent Si_3N_4 film cracks. **b**, Photograph of Si_3N_4 photonic chips, which are $5\times5\,mm^2$ in size, in comparison with a 1 cent Euro coin. The chip colour is a result of light interference caused by the SiO_2 cladding. **c**, Histogram of the intrinsic loss $\kappa_0/2\pi$ of 21,123 resonances. The most probable value is $\kappa_0/2\pi = 8.5$ MHz, corresponding to $Q_0 = 23\times10^6$ and a linear loss of 1.4 dB m^{-1}. **d**, Top: fitted microresonator dispersion $D_{int}/2\pi$, with $D_1/2\pi = 19.6$ GHz and $D_2/2\pi = 63.3$ kHz, relative to the reference resonance at the wavelength $\lambda_p = 1{,}559.4$ nm. Bottom: resonance frequency deviation from a D_2-dominant parabolic profile, defined as $(D_{int} - D_2\mu^2/2)/2\pi$, to outline mode crossings and $D_3/2\pi = -15$ Hz. Mode crossings well below 50 MHz are revealed due to the high resonance Q (loaded linewidth $\kappa/2\pi = 18$ MHz).

spectral range (FSR) resonators with Q exceeding 10×10^6 have been demonstrated[31]. However, spatial mode coupling in numerous waveguide bending sections significantly enhances avoided mode crossings in these microresonators, and probably prohibits single soliton formation. In addition, thermal effects in Si_3N_4 lead to short 'soliton steps'[23,32], which make the (single) soliton more difficult to access via simple laser frequency tuning. Complex techniques[33] can be used to overcome this challenge at the expense of requiring additional electronic and optical components. Here, we overcome the abovementioned challenges and demonstrate integrated Si_3N_4 soliton microcombs operating in the microwave X- and K-bands. We use these solitons to generate low-noise microwave signals, which could be utilized for radar and the next generation of wireless networks.

Principle and sample description

The principle of microwave generators based on integrated soliton microcombs is depicted in Fig. 1a. A photonic integrated microresonator is driven by a near-infrared continuous-wave (c.w.) laser to produce a soliton pulse stream, which, upon photodetection, generates a microwave signal whose frequency depends on the microresonator FSR. The key challenge here is to generate soliton pulses in centimetre-scale, macroscopic resonators made of integrated waveguides featuring sub-nanometre surface roughness. We overcome this challenge by using the photonic Damascene reflow process[34,35], which allows scalable manufacturing of high-Q integrated microresonators based on ultra-low-loss Si_3N_4 waveguides (linear propagation loss $\alpha \approx 1.4\,dB\,m^{-1}$) with high fabrication yield and reproducibility. Several key fabrication techniques are used, including deep-ultraviolet (DUV) stepper lithography based on 248 nm KrF excimer lasers to pattern the waveguides with reduced stitching errors and superior quality (see Methods), and stress-release patterns[34] to prevent crack formation in thick Si_3N_4 films required for anomalous group velocity dispersion (GVD). Additionally, to minimize spatial mode coupling between the soliton mode and other waveguide modes, we designed the microresonators in a perfect circular shape, with diameters of 2.30 mm and 4.60 mm for 20 and 10 GHz FSR, respectively. Figure 1b presents a photograph of the final Si_3N_4 photonic chips ($5\times5\,mm^2$ size).

The microresonator dispersion and the resonance linewidths in the fundamental transverse electric (TE_{00}) mode are characterized using the method described in ref. [35]. The microresonator dispersion is defined as $D_{int}(\mu) \equiv \omega_\mu - \omega_0 - D_1\mu = D_2\mu^2/2 + D_3\mu^3/6 + ...$, where $\omega_\mu/2\pi$ is the frequency of the μth resonance relative to the pump resonance $\omega_0/2\pi$, $D_1/2\pi$ corresponds to the FSR, $D_2/2\pi$ is the GVD and $D_3/2\pi$ is the third-order dispersion. For each resonance fit, the loaded linewidth $\kappa/2\pi = (\kappa_0 + \kappa_{ex})/2\pi$, intrinsic loss $\kappa_0/2\pi$ and coupling strength $\kappa_{ex}/2\pi$ are extracted. Figure 1c presents a histogram of $\kappa_0/2\pi$ for 21,123 fitted resonances from 14 characterized 10 GHz FSR chips. The most probable value is $\kappa_0/2\pi = 8.5$ MHz, corresponding to a statistical intrinsic quality factor of $Q_0 = 23\times10^6$. Figure 1d shows the measured $D_{int}/2\pi$ and outlines the resonance frequency deviation from a D_2-dominant parabolic profile, defined as $(D_{int} - D_2\mu^2/2)/2\pi$, so as to reveal mode crossings and the D_3 component. As evidenced in Fig. 1d, our fabrication and design yield an ideal anomalous GVD with significantly reduced mode crossings compared with previous work[30,31]. Details concerning chip input/output coupling and resonator coupling are presented in the Methods.

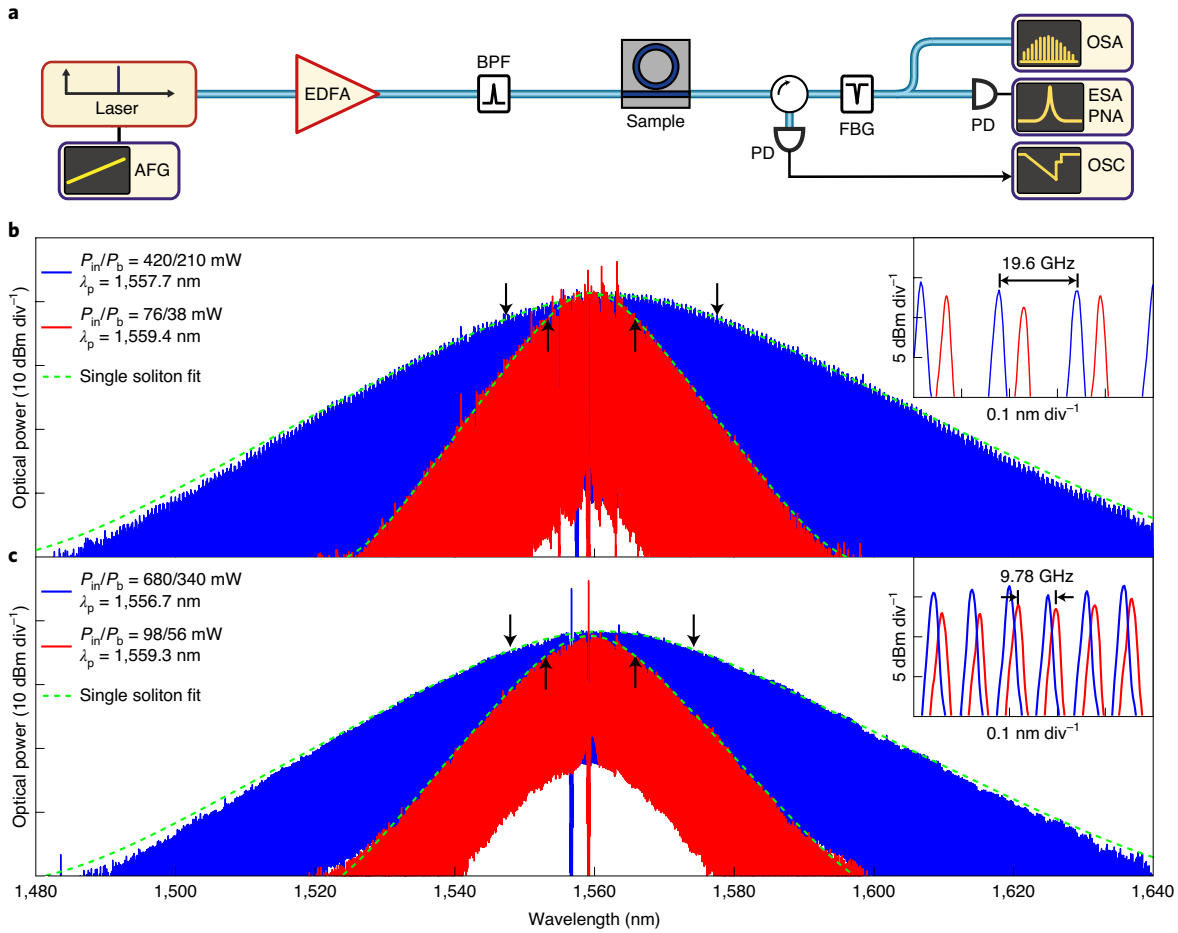

Fig. 2 | Single solitons with microwave K- and X-band repetition rates. a, Experimental set-up to generate solitons and to characterize the soliton phase noise. EDFA, erbium-doped fibre amplifier; AFG, arbitrary function generator; BPF, bandpass filter; FBG, fibre Bragg grating; OSA, optical spectrum analyser; OSC, oscilloscope; PD, photodiode; ESA/PNA, electrical spectrum analyser/phase noise analyser. **b**, Single soliton spectra for a 19.6 GHz repetition rate and 38 mW power in sample A (red, 3 dB bandwidth of 11.0 nm) and 210 mW power in sample B (blue, 3 dB bandwidth of 26.9 nm) and soliton spectrum fit (green dashed line). Arrows mark the 3 dB bandwidths, which contain 69 (red) and 170 (blue) comb lines, respectively. Inset: spectrum magnified view showing the 19.6 GHz mode spacing. **c**, Single soliton spectra for a 9.78 GHz repetition rate with 56 mW power in sample C (red, 3 dB bandwidth of 12.5 nm) and 340 mW power in sample D (blue, 3 dB bandwidth of 25.8 nm) and soliton spectrum fit (green dashed line). Arrows mark the 3 dB bandwidths, which contain 158 (red) and 327 (blue) comb lines, respectively. Inset: spectrum magnified view showing the 9.78 GHz mode spacing. Note that for the soliton spectra in **b** and **c**, a BPF is used to filter out the EDFA's amplified spontaneous emission noise in the pump laser, and an FBG is used to filter out the pump laser in the soliton spectra. P_{in}, input optical power to the chip; P_b, on-chip power in the bus waveguide.

K- and X-band soliton generation

Using the Damascene reflow process, we fabricated microresonators of FSR in the microwave K- and X-bands (for sample information see Methods). Using the set-up shown in Fig. 2a, single solitons are generated via simple laser piezo frequency tuning[23,36], in all tested samples. As shown in Fig. 2b, in sample A (red), the single soliton is generated with 38 mW power in the bus waveguide on-chip (76 mW power in the input lensed fibre), while parametric oscillation is observed at 7 mW. The single soliton spectrum fit shows a 3 dB bandwidth of 11.0 nm, corresponding to a pulse duration of 232 fs. This achievement of a single soliton with a K-band repetition rate features an extremely low threshold power, on par with the power values in silica and crystalline microresonators. This power level is compatible with state-of-the-art integrated lasers[37,38], creating a realistic prospect for fully integrated microcomb devices, especially in conjunction with resonator actuators (such as piezoelectric actuators[28] or metallic heaters[27]) to tune or stabilize the operation frequency. In sample B, the single soliton is generated with 210 mW power, and features 170 comb lines within the 3 dB bandwidth of 26.9 nm (94.6 fs pulse duration), ideal for creating dense wavelength-division multiplexing (WDM) channels for coherent communications[39]. We also generate single solitons at a 9.78 GHz repetition rate in the X-band, as shown in Fig. 2c, with a power of 56 mW in sample C (red) and 340 mW in sample D (blue). The 3 dB bandwidths are 12.5 nm (red, 158 comb lines, 203 fs pulse duration) and 25.8 nm (blue, 327 comb lines, 98.6 fs pulse duration), respectively. We further study the minimum power for multi-soliton generation in these samples, which is 22 mW for the 19.6 GHz rate in sample A and 32 mW for the 9.78 GHz rate in sample C (for the optical spectra see Supplementary Information).

Phase noise characterization

Next, we systematically analyse the phase fluctuations of the soliton-based K- and X-band microwave carriers. The measurement set-up is shown in Fig. 2a. The soliton pulse stream is driven by a c.w. diode laser (Toptica CTL). After the microresonator, the excess c.w. pump is rejected using a narrow-band optical notch filter before photodetection of the soliton repetition rate on a fast InGaAs

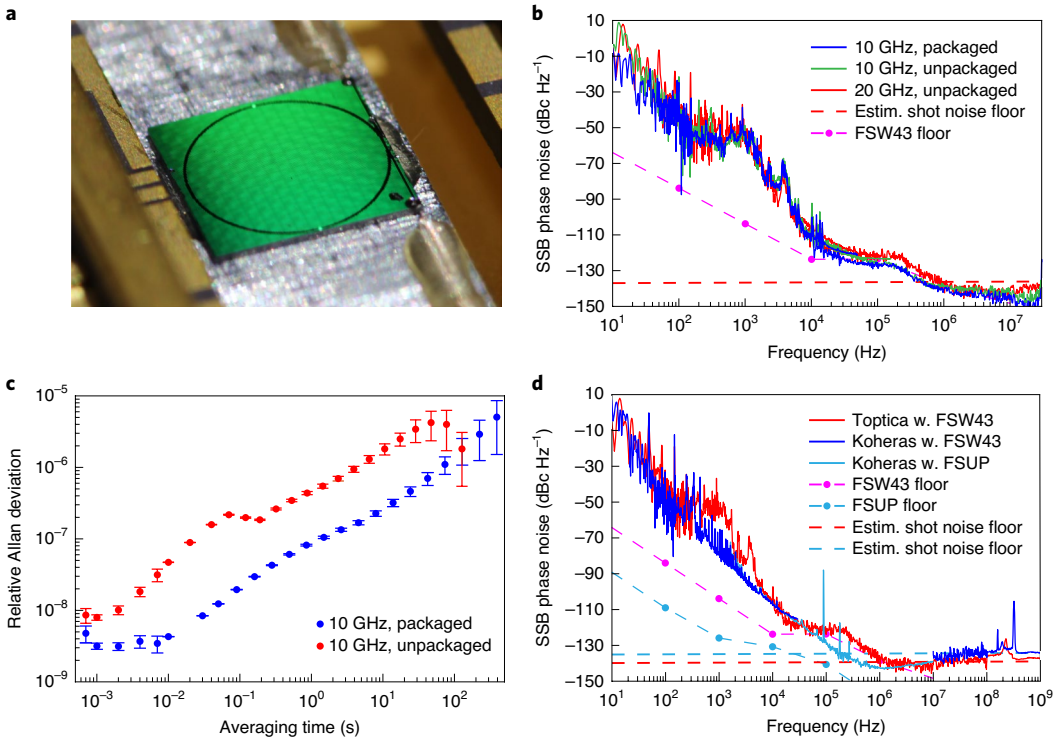

Fig. 3 | Phase noise characterization of the soliton repetition rate. a, Photograph of a packaged Si_3N_4 chip for X-band soliton generation, with input and output fibres glued to the chip. **b**, Comparison of free-running soliton phase noise using packaged (blue) and unpackaged (green) X-band soliton chips and an unpackaged K-band soliton chip (red). **c**, Measured relative Allan deviation of the X-band soliton repetition rate before (red) and after (blue) packaging the same chip, revealing the stability improvement. The error bars mark the confidence interval. **d**, Single-sideband (SSB) phase noise measured with the stabilized cavity–pump detuning at $\delta\omega/2\pi = 400$ MHz, using different lasers and PNAs (the noise floors of FSW43 and FSUP are indicated). The estimated shot noise floors are −140 dBc Hz^{-1} with the Toptica laser (red dashed line) and −135 dBc Hz^{-1} with the Koheras laser (blue dashed line).

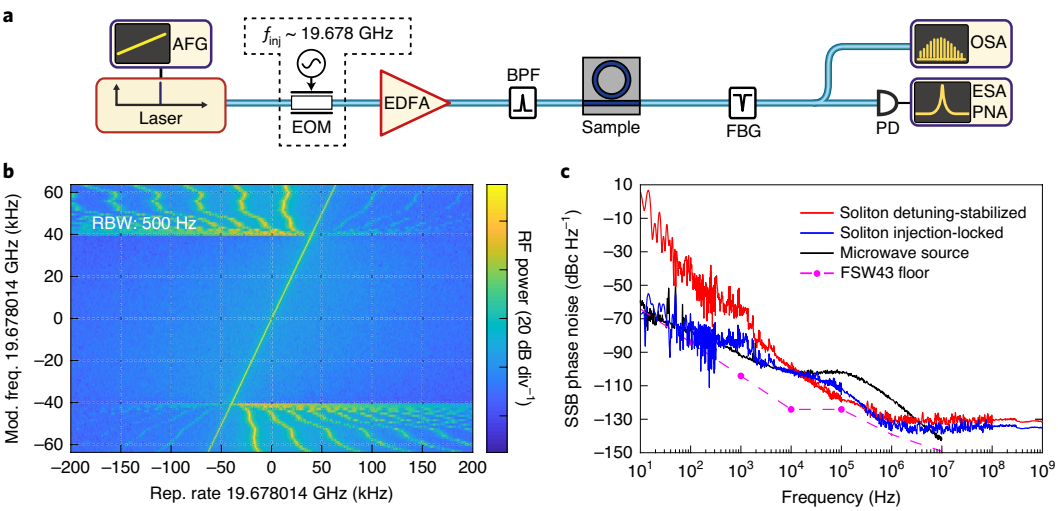

Fig. 4 | Soliton injection-locking to an external microwave source. a, Experimental set-up for soliton injection-locking. EOM, electro-optic modulator. **b**, Microwave spectrum evolution showing injection-locking of the soliton repetition rate f_{rep} with the modulation frequency f_{inj} on the c.w. pump, when $|f_{rep} - f_{inj}| < 40$ kHz. RBW, resolution bandwidth. **c**, SSB phase noise spectrum comparison of the injection-locked soliton (blue), the microwave source used to discipline the soliton (black) and the soliton with stabilized cavity–pump detuning (red). The soliton spectral purification effect is revealed above 10 kHz offset Fourier frequency.

photodiode (Discovery Semiconductors, DSC40). The output electrical signal of the photodiode is fed to a phase noise analyser (PNA; Rohde & Schwarz, FSW43). The soliton repetition rates around 9.78 GHz are characterized in the free-running state; that is, neither the laser frequency and power nor the microresonator is actively stabilized. A frequency modulation with a rate of ~5 Hz is observed (see Supplementary Information). This modulation is caused by unstable chip coupling from using suspended lensed fibres, which

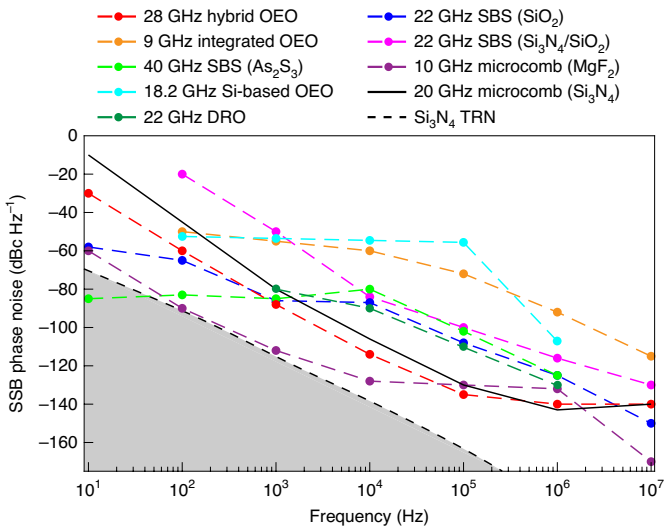

Fig. 5 | Comparison of compact photonics-based microwave generators. Performances of a 28 GHz hybrid optoelectronic oscillator (OEO; OEwaves HI-Q Nano-OEO), a 9 GHz integrated OEO[47], a 40 GHz OEO using stimulated Brillouin scattering (SBS) in As_2S_3 chalcogenide[48], an 18.2 GHz silicon-based OEO[49], a 22 GHz DRO (Microwave Dynamics DRO-1500), a 22 GHz SBS in SiO_2 (ref. [50]), a 22 GHz SBS in Si_3N_4/SiO_2 (ref. [51]), a 10 GHz microcomb in MgF_2 (ref. [14]) and a 20 GHz microcomb in Si_3N_4 (this work). The region below the fundamental limit imposed by TRN in Si_3N_4 (dashed black line) is shaded in grey.

are susceptible to vibrations. To increase the coupling stability, we glue fibres to the chip using a photonic packaging technique[40], as shown in Fig. 3a. A comparison of the relative Allan deviation before and after packaging the same 9.78 GHz FSR chip, depicted in Fig. 3c, proves that the chip packaging improves soliton stability.

Figure 3b shows the measured free-running phase noise of the 9.78 GHz soliton repetition rate before and after packaging the same chip, in comparison with the phase noise of a K-band soliton in an unpackaged 19.6 GHz FSR chip. Note that, in the case of the unpackaged 19.6 GHz soliton, although lensed fibres are used to couple light into and out of the chip, the power transmitted through the chip is actively stabilized (see Methods) to mimic the case of a packaged chip with stable fibre-chip coupling. Packaging clearly reduces the microwave phase noise at offset Fourier frequencies below 30 Hz, but at higher offset frequencies the phase noise reduction is minimum. Furthermore, no prominent phase noise difference is observed between the unpackaged 19.6 and 9.78 GHz solitons. In the following we focus only on the unpackaged 19.6 GHz soliton to further investigate the source of the observed phase noise.

To investigate the role of laser noise in the generated microwave signal, the laser phase noise is measured and correlated with the soliton repetition rate noise. The conversion of optical to microwave noise is estimated as −55 dB (see Supplementary Information). When the soliton is driven by a Toptica laser, as shown by the red curves in Fig. 3b,d, the noise feature within 100 Hz–10 kHz offset frequency is caused by the Toptica laser phase noise, while the step-like feature within 20 kHz–1 MHz is caused by the FSW43 PNA noise floor. In a different case, when the soliton is driven by a fibre laser (Koheras AdjustiK) featuring a lower phase noise level, the soliton phase noise is reduced as shown by the blue curve in Fig. 3d. An additional PNA (Rohde & Schwarz FSUP, with cross-correlations) is used here to overcome the FSW43 device limitation; however, this results in the phase noise in the 200 kHz–10 MHz range falling marginally below the shot noise floor, probably caused by parasitic anticorrelation effects in the FSUP PNA[41]. Our analysis shows that, when using the fibre laser, the main limitation for the soliton phase noise is the laser relative intensity noise (RIN) for offset frequencies below 1 MHz, with a contribution from the impact of thermo-refractive noise (TRN)[42] in Si_3N_4 on the cavity–pump detuning at offset frequencies in the 10–100 kHz range (see Supplementary Information). The absolute single-sideband (SSB) phase noise power spectral density of the microwave carrier reaches −80 dBc Hz^{-1} at 1 kHz offset Fourier frequency, −110 dBc Hz^{-1} at 10 kHz and −130 dBc Hz^{-1} at 100 kHz. Our current soliton phase noise performance is mainly limited by the pump lasers, so further phase noise reduction can be achieved by using lasers with lower phase noise and RIN. Finally, another solution to reduce the phase noise is to operate the soliton at a 'quiet point'[43], as explained in the Supplementary Information.

Soliton injection-locking

The low soliton repetition rate achieved in our work allows soliton injection-locking to an external microwave source[44], which can discipline the soliton repetition rate and improve long-term soliton stability, as is critical for applications requiring a stable and referenced comb line spacing. The modified experimental set-up is shown in Fig. 4a. Phase modulation is applied on the c.w. pump laser with a sweeping frequency f_{inj} around 19.6780 GHz. The evolution of the microwave spectrum of the soliton repetition rate with the sweeping f_{inj} is recorded as shown in Fig. 4b. The soliton injection-locking—that is, synchronization of the soliton repetition rate f_{rep} to the modulation frequency f_{inj}—is observed when $|f_{rep} - f_{inj}| < 40$ kHz. This injection-locking range marks a 100-fold increase compared to a previous demonstration in MgF_2 resonators (~300 Hz)[44]. The phase noise spectra of the injection-locked soliton (blue), the microwave source (black) and the soliton with a stabilized cavity–pump detuning (red, described in the Methods) are compared in Fig. 4c. The phase noise of the injection-locked soliton closely follows the microwave source's phase noise at an offset frequency below 10 kHz, apart from a residual bump at 1 kHz that originates from the pump laser. For offset Fourier frequencies above 10 kHz, the soliton-induced spectral purification effect is revealed, as the soliton phase noise departs from the injected microwave phase noise and becomes similar to the case with only active cavity–pump detuning stabilization.

Conclusion and outlook

In summary, we have demonstrated integrated soliton microcombs operating in the key microwave K- and X-bands, with pump power levels compatible with integrated lasers[37,38]. The low soliton repetition rate achieved here is intrinsically beneficial for dense WDM channel generation schemes[39] and could greatly reduce the system complexity of recently demonstrated soliton-based integrated frequency synthesizers[45] and atomic clocks[46]. Equally important, these soliton microcombs are promising building blocks for low-noise microwave generation. Figure 5 compares our soliton-based microwave generator to other compact photonics-based microwave generators[14,47–51] and a commercial GaN dielectric resonator oscillator (DRO)[52], as well as the limit imposed by TRN in Si_3N_4. The measured phase noise in our work is still 30 dB higher than the fundamental TRN limit (see Supplementary Information), revealing the considerable potential for further phase noise reduction, which can be achieved by using lasers with suppressed phase noise and RIN, and microresonators of higher Q. Although DROs still have better performance in terms of phase noise level and device size, integrated soliton microcombs could be a competitive solution for low-noise microwave generation on chip, with future advances in high-power, ultra-low-noise integrated lasers and fast photodiodes. Moreover, solitons are coherent multi-carrier optical sources where the microwave signal is naturally encoded into optical carriers, thus allowing the distribution of microwave signals directly via

optical fibres. Therefore, our results represent a step towards fully integrated soliton microcomb devices for low-noise optical and microwave synthesis in future architectures of radar and information-processing networks.

Online content

Any methods, additional references, Nature Research reporting summaries, source data, extended data, supplementary information, acknowledgements, peer review information; details of author contributions and competing interests; and statements of data and code availability are available at https://doi.org/10.1038/s41566-020-0617-x.

Received: 13 May 2019; Accepted: 4 March 2020;
Published online: 20 April 2020

References

1. Hecht, J. The bandwidth bottleneck that is throttling the Internet. *Nature* **536**, 139–142 (2016).
2. Capmany, J. & Novak, D. Microwave photonics combines two worlds. *Nat. Photon.* **1**, 319–330 (2007).
3. Supradeepa, V. et al. Comb-based radiofrequency photonic filters with rapid tunability and high selectivity. *Nat. Photon.* **6**, 186–194 (2012).
4. Ghelfi, P. et al. A fully photonics-based coherent radar system. *Nature* **507**, 341–345 (2014).
5. Khilo, A. et al. Photonic ADC: overcoming the bottleneck of electronic jitter. *Opt. Express* **20**, 4454–4469 (2012).
6. Lim, C. et al. Fiber-wireless networks and subsystem technologies. *J. Lightw. Technol.* **28**, 390–405 (2010).
7. Khan, M. H. et al. Ultrabroad-bandwidth arbitrary radiofrequency waveform generation with a silicon photonic chip-based spectral shaper. *Nat. Photon.* **4**, 117–122 (2010).
8. Ataie, V., Esman, D., Kuo, B.-P., Alic, N. & Radic, S. Subnoise detection of a fast random event. *Science* **350**, 1343–1346 (2015).
9. Temprana, E. et al. Overcoming Kerr-induced capacity limit in optical fiber transmission. *Science* **348**, 1445–1448 (2015).
10. Riehle, F. Optical clock networks. *Nat. Photon.* **11**, 25–31 (2017).
11. Rappaport, T. S., Murdock, J. N. & Gutierrez, F. State of the art in 60-GHz integrated circuits and systems for wireless communications. *Proc. IEEE* **99**, 1390–1436 (2011).
12. Xie, X. et al. Photonic microwave signals with zeptosecond-level absolute timing noise. *Nat. Photon.* **11**, 44–47 (2016).
13. Li, J., Yi, X., Lee, H., Diddams, S. A. & Vahala, K. J. Electro-optical frequency division and stable microwave synthesis. *Science* **345**, 309–313 (2014).
14. Liang, W. et al. High spectral purity Kerr frequency comb radio frequency photonic oscillator. *Nat. Commun.* **6**, 8957 (2015).
15. Marpaung, D., Yao, J. & Capmany, J. Integrated microwave photonics. *Nat. Photon.* **13**, 80–90 (2019).
16. Kippenberg, T. J., Gaeta, A. L., Lipson, M. & Gorodetsky, M. L. Dissipative Kerr solitons in optical microresonators. *Science* **361**, eaan8083 (2018).
17. Gaeta, A. L., Lipson, M. & Kippenberg, T. J. Photonic-chip-based frequency combs. *Nat. Photon.* **13**, 158–169 (2019).
18. Torres-Company, V. & Weiner, A. M. Optical frequency comb technology for ultra-broadband radio-frequency photonics. *Laser Photon. Rev.* **8**, 368–393 (2014).
19. Wu, J. et al. RF photonics: an optical microcombs' perspective. *IEEE J. Sel. Top. Quantum Electron.* **24**, 1–20 (2018).
20. Xu, X. et al. Broadband microwave frequency conversion based on an integrated optical micro-comb source. *J. Lightw. Technol.* **38**, 332–338 (2019).
21. Moss, D. J., Morandotti, R., Gaeta, A. L. & Lipson, M. New CMOS-compatible platforms based on silicon nitride and Hydex for nonlinear optics. *Nat. Photon.* **7**, 597–607 (2013).
22. Gyger, F. et al. Observation of stimulated Brillouin scattering in silicon nitride integrated waveguides. *Phys. Rev. Lett.* **124**, 013902 (2020).
23. Herr, T. et al. Temporal solitons in optical microresonators. *Nat. Photon.* **8**, 145–152 (2014).
24. Leo, F. et al. Temporal cavity solitons in one-dimensional Kerr media as bits in an all-optical buffer. *Nat. Photon.* **4**, 471–476 (2010).
25. Stern, B., Ji, X., Okawachi, Y., Gaeta, A. L. & Lipson, M. Battery-operated integrated frequency comb generator. *Nature* **562**, 401–405 (2018).
26. Raja, A. S. et al. Electrically pumped photonic integrated soliton microcomb. *Nat. Commun.* **10**, 680 (2019).
27. Joshi, C. et al. Thermally controlled comb generation and soliton modelocking in microresonators. *Opt. Lett.* **41**, 2565–2568 (2016).
28. Tian, H. et al. Hybrid integrated photonics using bulk acoustic resonators. Preprint at https://arxiv.org/abs/1907.10177 (2019).
29. Yang, K. Y. et al. Bridging ultrahigh-*Q* devices and photonic circuits. *Nat. Photon.* **12**, 297–302 (2018).
30. Johnson, A. R. et al. Chip-based frequency combs with sub-100 GHz repetition rates. *Opt. Lett.* **37**, 875–877 (2012).
31. Xuan, Y. et al. High-*Q* silicon nitride microresonators exhibiting low-power frequency comb initiation. *Optica* **3**, 1171–1180 (2016).
32. Li, Q. et al. Stably accessing octave-spanning microresonator frequency combs in the soliton regime. *Optica* **4**, 193–203 (2017).
33. Stone, J. R. et al. Thermal and nonlinear dissipative-soliton dynamics in Kerr-microresonator frequency combs. *Phys. Rev. Lett.* **121**, 063902 (2018).
34. Pfeiffer, M. H. P. et al. Photonic Damascene process for integrated high-*Q* microresonator based nonlinear photonics. *Optica* **3**, 20–25 (2016).
35. Liu, J. et al. Ultralow-power chip-based soliton microcombs for photonic integration. *Optica* **5**, 1347–1353 (2018).
36. Guo, H. et al. Universal dynamics and deterministic switching of dissipative Kerr solitons in optical microresonators. *Nat. Phys.* **13**, 94–102 (2016).
37. Morton, P. A. & Morton, M. J. High-power, ultra-low noise hybrid lasers for microwave photonics and optical sensing. *J. Lightw. Technol.* **36**, 5048–5057 (2018).
38. Huang, D. et al. High-power sub-kHz linewidth lasers fully integrated on silicon. *Optica* **6**, 745–752 (2019).
39. Mazur, M. et al. Enabling high spectral efficiency coherent superchannel transmission with soliton microcombs. Preprint at https://arxiv.org/abs/1812.11046 (2018).
40. Raja, A. S. et al. Chip-based soliton microcomb module using a hybrid semiconductor laser. *Opt. Express* **28**, 2714–2721 (2020).
41. Nelson, C. W., Hati, A. & Howe, D. A. A collapse of the cross-spectral function in phase noise metrology. *Rev. Sci. Instrum.* **85**, 024705 (2014).
42. Huang, G. et al. Thermorefractive noise in silicon-nitride microresonators. *Phys. Rev. A* **99**, 061801 (2019).
43. Yi, X. et al. Single-mode dispersive waves and soliton microcomb dynamics. *Nat. Commun.* **8**, 14869 (2017).
44. Weng, W. et al. Spectral purification of microwave signals with disciplined dissipative Kerr solitons. *Phys. Rev. Lett.* **122**, 013902 (2019).
45. Spencer, D. T. et al. An optical-frequency synthesizer using integrated photonics. *Nature* **557**, 81–85 (2018).
46. Newman, Z. L. et al. Architecture for the photonic integration of an optical atomic clock. *Optica* **6**, 680–685 (2019).
47. Tang, J. et al. Integrated optoelectronic oscillator. *Opt. Express* **26**, 12257–12265 (2018).
48. Merklein, M. et al. Widely tunable, low phase noise microwave source based on a photonic chip. *Opt. Lett.* **41**, 4633–4636 (2016).
49. Do, P. T. et al. Wideband tunable microwave signal generation in a silicon-based optoelectronic oscillator. Preprint at https://arxiv.org/abs/1903.01137 (2019).
50. Li, J., Lee, H. & Vahala, K. J. Microwave synthesizer using an on-chip Brillouin oscillator. *Nat. Commun.* **4**, 2097 (2013).
51. Gundavarapu, S. et al. Sub-hertz fundamental linewidth photonic integrated Brillouin laser. *Nat. Photon.* **13**, 60–67 (2019).
52. Rice, P. et al. A 10 GHz dielectric resonator oscillator using GaN technology. *2004 IEEE MTT-S International Microwave Symposium Digest* **3**, 1497–1500 (2004).

Methods

DUV stepper lithography. The advantages of DUV stepper lithography over electron-beam lithography (EBL), besides the higher yield and lower cost, are as follows: (1) the stitching errors on the wafer are four or five times smaller than the ones on the reticle used in the industrial-standard four- or five-demagnification-lens systems; (2) the reticle writing using standard photolithography (~1 h) is much faster than wafer writing using EBL (>10 h), so the field-to-field (or stripe-to-stripe) time delay is significantly shorter with DUV than with EBL, leading to smaller stitching errors caused by beam drift; (3) the field (or stripe) size of photolithography for reticle writing is much larger than the field size of EBL for wafer writing, leading to fewer stitching errors; (4) multipass for reticle writing can be easily adapted with reasonable cost increases. Consequently, DUV stepper lithography can provide superior lithography quality and has been used for recently demonstrated integrated Brillouin lasers[51] based on low-confinement Si_3N_4 waveguides with optical propagation loss below 1 dB m^{-1} (refs. [53,54]).

Sample information. More than 20 samples were tested and single solitons were generated in every sample. Only four selected samples (A, B, C and D) are shown here. Samples A and B were used to generate the solitons with 19.6 GHz repetition rate, as shown in Fig. 2b. Sample A is undercoupled, with a loaded linewidth of $\kappa/2\pi = 18$ MHz and coupling coefficient of $\eta \equiv \kappa_{ex}/\kappa \approx 1/3$. Sample B is overcoupled, with $\kappa/2\pi = 27$ MHz and $\eta \approx 2/3$. The soliton generated in sample B was used for the K-band soliton phase noise characterization. Samples C and D were used to generate the solitons with 9.78 GHz repetition rate, as shown in Fig. 2c. Sample C is undercoupled, with $\kappa/2\pi = 14$ MHz and $\eta \approx 2/5$. The soliton generated in sample C was used for the X-band soliton phase noise characterization. Sample D is overcoupled, with $\kappa/2\pi = 22$ MHz and $\eta \approx 2/3$. The waveguide cross-sections, width × height, were $1.70 \times 0.95\ \mu m^2$ for samples A and B and $2.10 \times 0.95\ \mu m^2$ for samples C and D, respectively. A Raman self-frequency shift[55,56] of ~4.9 nm was observed in sample B and ~4.4 nm in sample D. The c.w.-to-single-soliton power conversion efficiency was ~0.4% in sample A and ~0.2% in sample C.

Coupling scheme. The microresonator was coupled to a multi-mode bus waveguide of the same cross-section to achieve high coupling ideality[57]. Both straight and pulley bus waveguides were studied in this work, but no prominent performance difference was observed. Light was coupled into and out of the chip device via double-inverse nanotapers[58]. The coupling loss was ~3 dB per facet, corresponding to ~25% fibre–chip–fibre coupling efficiency.

Auxiliary soliton stabilization technique. To improve soliton stability throughout the experiment without gluing the fibres to the chip, two auxiliary soliton stabilization schemes were implemented in our work. The first method stabilized the transmitted power through the chip using an acousto-optic modulator (varying the pump power), and a power servo based on a proportional-integral-derivative (PID) controller was used to keep the power constant at the chip output. The second method actively stabilized the cavity–pump detuning using an offset-sideband Pound–Drever–Hall lock[33] with feedback applied to the pump laser power, which can effectively compensate the cavity resonance jitter induced by coupling fluctuations (for a description of the stabilization set-up see Supplementary Information). Two cases are investigated in Fig. 3d. In case A, with power stabilization, the soliton was driven by a diode laser (Toptica) and the FSW43 PNA was used. In case B, with detuning stabilization, the soliton was driven by a fibre laser (Koheras AdjustiK), and, besides the FSW43, the FSUP was used only for the 10 kHz–1 MHz offset frequency range. Note that, due to the fact that our current soliton phase noise is mainly limited by the laser used (laser phase noise or RIN), applying these soliton stabilization schemes does not necessarily result in prominent soliton phase noise reduction.

Data availability

The data that support the plots within this paper and other findings of this study are available on Zenodo (https://doi.org/10.5281/zenodo.3666737). All other data used in this study are available from the corresponding author upon reasonable request.

References

53. Bauters, J. F. et al. Planar waveguides with less than 0.1 dB/m propagation loss fabricated with wafer bonding. *Opt. Express* **19**, 24090–24101 (2011).
54. Spencer, D. T., Bauters, J. F., Heck, M. J. R. & Bowers, J. E. Integrated waveguide coupled Si_3N_4 resonators in the ultrahigh-*Q* regime. *Optica* **1**, 153–157 (2014).
55. Karpov, M. et al. Raman self-frequency shift of dissipative Kerr solitons in an optical microresonator. *Phys. Rev. Lett.* **116**, 103902 (2016).
56. Yi, X., Yang, Q.-F., Yang, K. Y. & Vahala, K. Theory and measurement of the soliton self-frequency shift and efficiency in optical microcavities. *Opt. Lett.* **41**, 3419–3422 (2016).
57. Pfeiffer, M. H. P., Liu, J., Geiselmann, M. & Kippenberg, T. J. Coupling ideality of integrated planar high-*Q* microresonators. *Phys. Rev. Appl.* **7**, 024026 (2017).
58. Liu, J. et al. Double inverse nanotapers for efficient light coupling to integrated photonic devices. *Opt. Lett.* **43**, 3200–3203 (2018).

Acknowledgements

We thank N. J. Engelsen, G. Huang, W. Weng, M. A. Anderson and S. A. Bhave for discussions. This work was supported by contract no. FA9550-19-C-7001 (KECOMO) from the Defense Advanced Research Projects Agency (DARPA), Microsystems Technology Office (MTO), by the Air Force Office of Scientific Research, Air Force Materiel Command, USAF under award no. FA9550-15-1-0250, and by the Swiss National Science Foundation under grant no. 176563 (BRIDGE) and no. 165933. E.L. and M.K. acknowledge support from the European Space Technology Centre under ESA contract nos. 4000116145/16/NL/MH/GM and 4000118777/16/NL/GM, respectively. J.H. acknowledges support provided by H.-Y. Tam and the General Research Fund of the Hong Kong Government under project PolyU 152207/15E. H.G. acknowledges support from the European Union's Horizon 2020 research and innovation programme under Marie Sklodowska-Curie IF grant no. 709249. The Si_3N_4 microresonator samples were fabricated in the EPFL Center of MicroNanoTechnology (CMi).

Author contributions

J.L. designed and fabricated the Si_3N_4 samples, with assistance from R.N.W. and H.G. Samples were characterized and analysed by J.L. and J.H. J.H., J.L., A.S.R. and M.K. performed the soliton generation experiment. E.L., A.S.R., J.R., J.L. and R.B. performed the phase noise measurements and the soliton injection-locking experiment. J.L., R.B., E.L. and T.J.K. wrote the manuscript, with input from the other authors. T.J.K. supervised the project.

Competing interests

The authors declare no competing interests.

Additional information

Supplementary information is available for this paper at https://doi.org/10.1038/s41566-020-0617-x.

Correspondence and requests for materials should be addressed to T.J.K.

Reprints and permissions information is available at www.nature.com/reprints.